

Enhancement of nominally-forbidden interband optical transitions in quantum dots

Gustavo A. Narvaez and Alex Zunger
National Renewable Energy Laboratory, Golden, Colorado 80401
(Dated: May 24, 2019)

We calculate the excitonic optical absorption spectra of (In,Ga)As/GaAs self-assembled quantum dots by adopting an atomistic pseudopotential approach to the single-particle problem followed by a configuration-interaction approach to the many-body problem. We find three types of *allowed* transitions that would be naively expected to be forbidden. (i) Transitions that are parity forbidden in simple effective mass models with infinite confining wells (e.g. 1S-2S, 1P-2P) but are enhanced by finite band-offsets and orbital-mixing effects; (ii) light-hole-to-conduction transitions, enabled by the confinement of light-hole states; and (iii) transitions that show and enhanced intensity due to electron-hole configuration mixing with allowed transitions. Transitions in (i) and (ii) may explain recently observed satellites of the allowed P - P transitions.

The interest in quantum dot spectroscopy stems, to a large extent, from the nature of their confined interband optical transitions. Yet, only rather simple theoretical approaches have been applied to discuss which transitions are formally allowed and which are formally forbidden. Here, we discuss the nature of confined transitions in lens-shaped (In,Ga)As/GaAs quantum dots by using an atomistic pseudopotential approach.^{1,2,3} Specifically, we study three mechanisms that render nominally-forbidden transitions, in lower approximations, to allowed transitions within more realistic approximations: (i) “2S-to-1S” and “2P-to-1P” “crossed” transitions allowed by finite band-offset effects and orbital mixing; (ii) Transitions involving a mixed heavy-hole and light-hole states, enhanced by the confinement of light-hole states; and (iii) many-body configuration-mixing intensity enhancement enabled by electron-hole Coulomb interaction.

In our approach, the atomistic single-particle energies \mathcal{E}_i and wave functions ψ_i are solutions to the atomistic Schrödinger equation¹

$$\{-\frac{1}{2}\nabla^2 + V_{SO} + \sum_{l,\alpha} v_\alpha(\mathbf{r} - \mathbf{R}_{l,\alpha})\}\psi_i = \mathcal{E}_i \psi_i, \quad (1)$$

where v_α is a pseudopotential for atom of type α , with

l -th site position $\mathbf{R}_{l,\alpha}$ in either the dot or the GaAs matrix. V_{SO} is a non-local (pseudo) potential that accounts for spin-orbit coupling.³ In the single-particle approximation, the transition intensity for light polarized along $\hat{\mathbf{e}}$ is

$$I^{(SP)}(\omega; \hat{\mathbf{e}}) = \sum_{i,j} |\langle \psi_i^{(e)} | \hat{\mathbf{e}} \cdot \mathbf{p} | \psi_j^{(h)} \rangle|^2 \delta[\hbar\omega - \mathcal{E}_i^{(e)} + \mathcal{E}_j^{(h)}], \quad (2)$$

where \mathbf{p} is the electron momentum.⁴

In addition to the single-particle effects, many-particle effects cause each of the monoexciton states $\Psi^{(\nu)}(X^0)$ to be a mixture of several electron-hole pair configurations (Slater determinants) $e_i h_j$. Namely,

$$|\Psi^{(\nu)}(X^0)\rangle = \sum_{i,j} C_{i,j}^{(\nu)} |e_i h_j\rangle. \quad (3)$$

The coefficients $C_{i,j}^{(\nu)}$ are determined by the degree of configuration mixing allowed by the electron-hole Coulomb and exchange interaction.⁵ This mixing is determined by the symmetry of the e - h orbitals and by their single-particle energy separation. The many-body optical absorption for (incoherent) unpolarized light is given by⁶

$$I^{(MP)}(\hbar\omega) = \frac{1}{3} \sum_{\nu} \left[\sum_{\hat{\mathbf{e}}=\hat{\mathbf{x}},\hat{\mathbf{y}},\hat{\mathbf{z}}} |\langle \Psi^{(\nu)}(X^0) | \hat{\mathbf{e}} \cdot \mathbf{p} | 0 \rangle|^2 \right] \delta[\hbar\omega - E^{(\nu)}(X^0)]. \quad (4)$$

Thus, the configuration mixing can make transitions that are forbidden in the single-particle single-band approximation become allowed in the many-particle representation of Eq. (4) by borrowing oscillator strength from bright transitions.

The calculated absorption spectra of self-assembled dots.—Figure 1 shows our calculated single-particle [Eq. (2); Fig. 1(a)] and many-particle [Eq. (4); Fig.

1(b)] absorption spectrum of X^0 for a lens-shaped $\text{In}_{0.6}\text{Ga}_{0.4}\text{As}/\text{GaAs}$ quantum dot with base diameter $b = 200$ Å and height $h = 20$ Å that confines two shells of electron states: $\{1S_e; 1P_e\}$. The energy of the transitions is shown as a shift $\Delta\mathcal{E}$ from the single-particle exciton gap $\mathcal{E}_0^{(e)} - \mathcal{E}_0^{(h)}$ [in Fig. 1(a)] or the ground-state energy of the monoexciton $E^{(0)}(X^0)$ [in Fig. 1(b)]. Figure 2

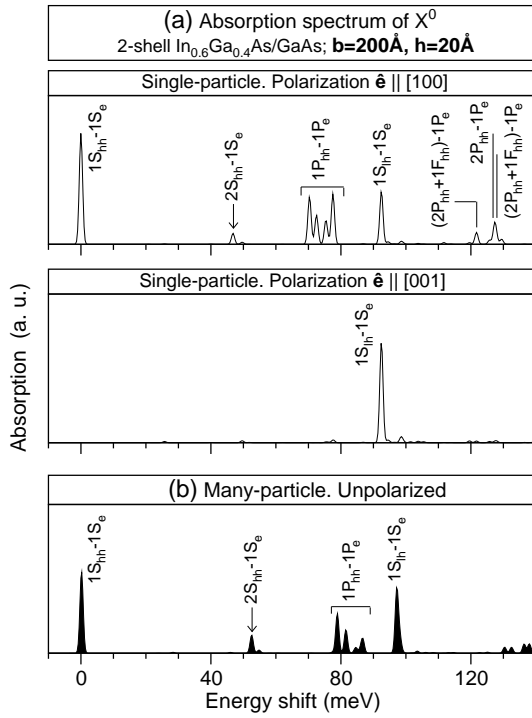


FIG. 1: Optical absorption spectrum of X^0 in a lens-shaped $\text{In}_{0.6}\text{Ga}_{0.4}\text{As}/\text{GaAs}$ quantum dot (base diameter $b = 200$ Å, height $h = 20$ Å) calculated at the (a) single-particle level of approximation [Eq. (2)] under in-plane ($\hat{e} \parallel [100]$; top) and out-of-plane ($\hat{e} \parallel [001]$; bottom) polarization; and (b) at the many-particle level [Eq. (4)] for unpolarized light. Labels indicate the electron-hole (leading) origin of the optical transitions, and their energy is shown relative to (a) the single-particle gap $\mathcal{E}_0^{(e)} - \mathcal{E}_0^{(h)} = 1333$ meV and (b) the ground-state energy $E^{(0)}(X^0) = 1309$ meV of X^0 .

shows equivalent results for two dots with $b = 252$ Å and heights $h = 20$ Å and 35 Å, which confine two $\{1S_e; 1P_e\}$ and three $\{1S_e; 1P_e; 1D_e + 2S_e\}$ shells of electron states, respectively.⁷ As expected, we find *nominally allowed* single-particle transitions, including (i) the fundamental transition $1S_{hh}-1S_e$ at $\Delta\mathcal{E} = 0$ meV; (ii) the $1P_{hh}-1P_e$ transitions with energy shifts $\Delta\mathcal{E} \sim 75$ meV and 65 meV for dots with $b = 200$ Å and 252 Å, respectively; and (iii) the transitions $1D_{hh}-1D_e$ and $2S_{hh}-2S_e$ at $\Delta\mathcal{E} \sim 130$ meV for the three-shell dot ($b = 252$ Å, $h = 35$ Å). Note that the underlying atomistic C_{2v} symmetry of the circular-base lens-shape dot splits the electron and hole $1P$ and $1D$ states into 3 and 5 levels, respectively, and causes these states to be a mixture of $L_z = \pm 1$ and $L_z = \pm 2$, respectively. [L_z is the projection of the angular momentum along the cylindrical ([001], out-of-plane) axis of the dot.] Thus, in contrast to predictions of simplified models that assume $C_{\infty v}$ shape symmetry, transitions involving states $1P$ and $1D$ are split into four and nine lines, respectively (Figs. 1 and 2). We next discuss the *nominally-forbidden* transitions.

(1) *Band-offset and orbital-mixing induced 1S-2S*

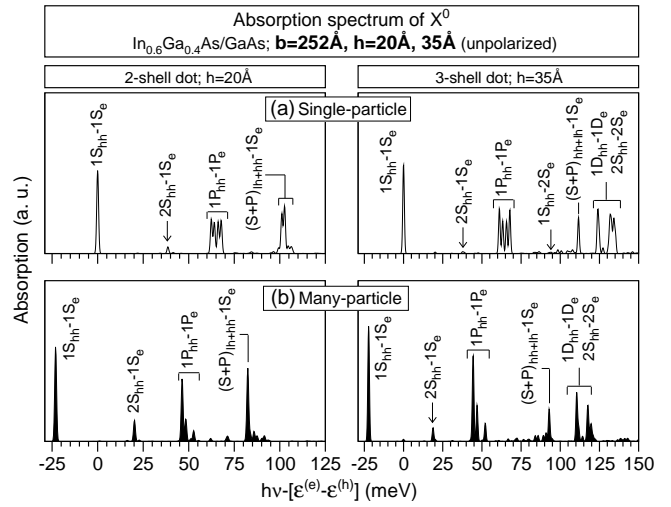


FIG. 2: *Idem* Fig. 1(b) for two $\text{In}_{0.6}\text{Ga}_{0.4}\text{As}/\text{GaAs}$ quantum dots that confine two (left panel) and three (right) shells of electron states, with heights $h = 20$ Å and 35 Å, respectively, and base $b = 252$ Å.

transitions.—If the electron and hole envelope wave functions are identical, the envelope-function selection rules indicate that only $\Delta i = 0$ ($i \rightarrow i$) transitions are allowed. This will be the case in the single-band effective mass approximation if the confinement potential (band offset between dot and environment) for electron and hole are infinite. This expectation that $2S_h-1S_e$ or $1S_h-2S_e$ as well as $2P_h-1P_e$ transitions are forbidden in the single-particle description is reflected in Refs. [8,9,10,11,12]. In contrast, we find a few $\Delta i \neq 0$ transitions with significant intensity: (i) $2S_{hh}-1S_e$ [Figs. 1(a) and 2(a)], which we find *below* $1P_{hh}-1P_e$; (ii) four transitions that involve the electron states $1P_e$ and hole states $2P_{hh}$ (also found in Ref. 13) and $2P_{hh}+1F_{hh}$ [Fig. 1(a)]; and (iii) transitions $1S_{hh}-2S_e$, and $2S_{hh}-1D_e$ and $1D_{hh}-2S_e$ in the three-shell dot (Fig. 2). The latter (D -shell) transitions arise from the mixing of $L_z = \pm 2$ and 0 present in the electron and hole wave functions. There are two reasons why $\Delta i \neq 0$ transitions are allowed. First, in the case of *finite* band offsets or, equivalently, when the electron and hole wavefunctions are not identical, the condition $\Delta i = 0$ is relaxed and transitions $j \rightarrow i$ may be allowed even in the effective-mass approximation. The latter happens to be the case in the work of Vasanelly *et al.* (Ref. 13) in which $2S_{hh}-1S_e$ and $2P_{hh}-1P_e$ transitions between confined electron and hole levels were found to have finite, non-negligible oscillator strength. Second, orbital mixing also makes such transition allowed: For example, a dot made of zinc-blende material and having a lens or cylindrical shape has the atomistic symmetry C_{2v} while spherical dots have T_d symmetry. In contrast, simplified continuum-like effective-mass based theories for dots use the symmetry of the *macroscopic shape* (lens, cylinder, sphere) rather than the true *atomistic* symmetry. For example, for zinc-blende lenses and cylinders one uses $C_{\infty v}$

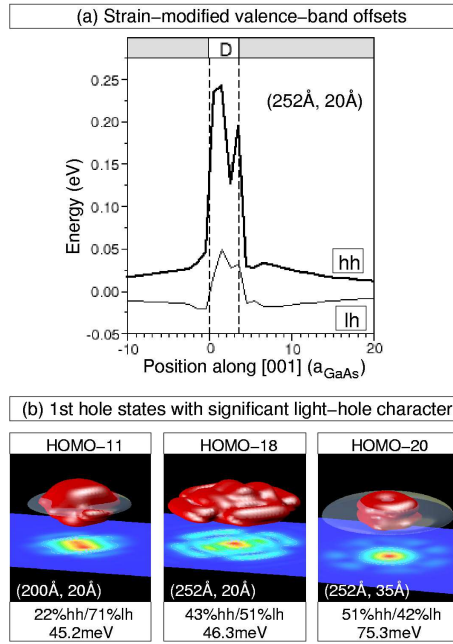


FIG. 3: (Color online) (a) First (thick line) and second (thin line) strain-modified valence-band offsets along a line $\parallel [001]$ that pierces a lens-shaped $\text{In}_{0.6}\text{Ga}_{0.4}\text{As}/\text{GaAs}$ quantum dot through its center. In the dot (D), the first and second offsets have heavy-hole (hh) and light-hole (lh) character, respectively, whereas in the barrier (grey area) these characters switch. (b) Wave functions of the first hole state with significant lh character for different $\text{In}_{0.6}\text{Ga}_{0.4}\text{As}/\text{GaAs}$ dots. Iso-surfaces enclose 75% of the charge density, while contours are taken at 1 nm above the base. The energy $\mathcal{E}_j^{(h)} - E_v(\text{GaAs})$ of the state appears in each panel. $E_v(\text{GaAs}) = -5.620$ eV is the GaAs VBM. The hh and lh character is indicated in percentages.

symmetry. In such continuum effective-mass approaches, transition $i-j$ is allowed as long as the overlap between the respective envelope functions is non-zero. For example, for spherical quantum dots one expects $S-S$ transitions to be allowed but not $D-S$ transitions. Yet, in the true point group symmetry of the *zinc-blende sphere* the highest occupied hole state has mixed $S+D$ symmetry, which renders transition $1S_h-1D_e$ allowed,^{14,15} and similarly the “ $2S-1S$ ” transition is allowed because the $2S_{hh}$ state also contains $1S_{hh}$ character.¹⁶

(2) *Strong light-hole-electron transitions.*—In *bulk* zinc-blende semiconductors the valence-band maximum is made of degenerate heavy-hole (hh , $|3/2, \pm 3/2\rangle$) and light-hole (lh , $|3/2, \pm 1/2\rangle$) states.¹⁷ While *both* optical transitions $hh-\Gamma_{1c}$ and $lh-\Gamma_{1c}$ are polarized in the $\hat{x}-\hat{y}$ plane, only the latter transition presents polarization along \hat{z} ($\parallel [001]$). Under biaxial strain these hh and lh states split. In bulk, the relative energy of these states and their splitting depend on the strain: for compressive (e.g. InAs on GaAs) the lh is below the hh while for tensile (e.g. GaAs on InAs) the lh is above the hh .¹⁸ In *quantum dots* the energy of lh states is unknown, but it is gen-

erally assumed to be unconfined; so, the $lh-\Gamma_{1c}$ transition is expected to be absent. Nonetheless, Minnaert *et al*¹⁹ have speculated that despite the compressive strain in InAs/GaAs dots the lh state is above the hh states, while Ribeiro *et al*²⁰ have suggested the presence of a lh -derived state *below* the hh states by measuring photo-reflectance and photo-absorption in (In,Ga)As/GaAs dots. Adler *et al*²¹ and Akimov *et al*²² have also suggested the presence of lh -derived transitions in photoluminescence excitation (PLE) experiments in InAs/GaAs and CdSe/ZnSe self-assembled quantum dots, respectively. We show in Fig. 3(a) the strain-modified valence-band offsets of a lens-shaped $\text{In}_{0.6}\text{Ga}_{0.4}\text{As}/\text{GaAs}$ dot with $b = 252$ Å and $h = 20$ Å, calculated along a line normal to the dot base that pierces the dot through its center. In agreement with Ribeiro *et al*²⁰, but in contrast with Minnaert *et al*¹⁹, within the dot the heavy-hole (hh) potential is above the light-hole (lh) one. Correspondingly, our atomistic pseudopotential calculations reveal weakly *confined* hole states with a significant lh character deeper than the hh state. The wave functions of the first of these states are shown in Fig. 3(b). These deep states visibly penetrate into the barrier—a feature remarkably prominent in the dot with $b = 252$ Å and $h = 20$ Å. The energy spacing between the highest hole state [HOMO ($\psi_0^{(h)}$)] and the deep lh -type states increases from 92.4 meV to 101.1 meV and 111.7 meV for HOMO-11 [$\psi_{11}^{(h)}$], HOMO-18 [$\psi_{18}^{(h)}$], and HOMO-20 [$\psi_{20}^{(h)}$], respectively. These states give rise to two lh -derived transitions in the absorption spectra: (i) $1S_{lh}-1S_e$ [Fig. 1] with the deep lh -type state being a mixture of 71% lh and 22% hh . As seen in Fig. 1, this transition has a large intensity in both $\hat{e} \parallel [100]$ and $\hat{e} \parallel [001]$ polarizations. (ii) $(S+P)_{lh+hh}-1S_e$ (Fig. 2) with hh/lh percentages of 43/51 and 51/42 for the two-shell and three-shell dots, respectively. In these dots with $b = 252$ Å, the larger base size reduces the spacing between confined hole states and promotes character mixing. In the 2-shell dot, the offset energy of this transition with respect to $1P_{hh}-1P_e$ is 36.0 meV, in excellent agreement with the observed value.²³

(3) *Coulomb-induced transitions that are forbidden in the single-particle description.*—Due to the electron-hole Coulomb interaction, each monoexciton state $\Psi(X^0)$ is a mixture of electron-hole configurations [Eq. (3)]. This mix results in a enhancement/diminiishment of the intensity of both allowed and nominally-forbidden transitions in the absorption spectra [Fig. 2(b)]. These are shown by comparing Fig. 1(a) *vs* Fig. 1(b) and Fig. 2(a) *vs* Fig. 2(b). The many-body effects include (i) enhancement of the intensity of the nominally forbidden transition $2S_{hh}-1S_e$ particularly in the 3-shell dot (Fig. 2); (ii) redistribution of the intensity of both the nominally allowed $1P_{hh}-1P_e$ transitions and the $1D_{hh}-1D_e$ and $2S_{hh}-2S_e$ transitions; and (iii) change of the intensity of the transitions involving deep hole states with significant light-hole character. The mixing enhancement $\eta(2S_{hh}-1S_e) = I^{(CI)}(2S_{hh}-1S_e)/I(2S_{hh}-1S_e) = 3.2$ and $\eta(1S_{hh}-1S_e) = 1.1$ for the 2-shell dot, while

$\eta(2S_{hh}-1S_e) = 8.2$ and $\eta(1S_{hh}-1S_e) = 1.3$ for the three shell dot. For both dots, the enhancement of transition $2S_{hh}-1S_e$ arises mainly from configuration mixing with the four configurations $|1P_{hh}1P_e\rangle$. The degree of mixing is *small*, $\sim 2\%$ for both dots, due to the *large* (~ 26 meV) energy splitting between these electron-hole configurations at the single-particle (non-interacting) level, yet sufficient to cause a sizeable enhancement of the intensity. We find that the larger $\eta(2S_{hh}-1S_e)$ for the 3-shell dot arises from a larger mixing with configuration $|1S_{hh}1S_e\rangle$.

Comparison with experiment: The calculated $2S_{hh}-1S_e$ transition is ~ 26 meV *below* the strongest $1P_{hh}-1P_e$ transition; in excellent agreement with those observed by Preisler *et al.*²³ in magneto-photoluminescence, who found 25 meV, and in contrast to the effective-mass approximation results of Vasanelli *et al.*, which place $2S_{hh}-1S_e$ *below* $1P_{hh}-1P_e$. The calculated $1S_{hh}-1S_e$ transition is 18.3 meV below $1P_{hh}-1P_e$, in only rough agreement with the value of 35 meV observed by Preisler *et al.*²³

The effect of configuration-mixing on the optical spectrum was previously discussed within the simplified single-band 2D-EMA parabolic model.^{9,10} Such continuum theories assume macroscopic shapes that lead to significant degeneracies among the single-particle states of Eq. (1): $1S$; $1P^{(+)} = 1P^{(-)}$ (twofold); and $1D^{(+)} = 1D^{(-)} = 2S$ (threefold). As a result, there is an artificially strong many-body mixing in Eq. (3). The many-particle exciton states with allowed Coulomb mixing are:

$$\begin{aligned} |\Psi_A\rangle &= |1S_{hh} 1S_e\rangle \\ |\Psi_B\rangle &= \frac{1}{\sqrt{2}}(|1P_{hh}^{(+)} 1P_e^{(+)}\rangle + |1P_{hh}^{(-)} 1P_e^{(-)}\rangle) \\ |\Psi_H\rangle &= \frac{1}{\sqrt{2}}(|2S_{hh} 1S_e\rangle + |1S_{hh} 2S_e\rangle) \\ |\Psi_D\rangle &= \frac{1}{\sqrt{3}}(|1D_{hh}^{(+)} 1D_e^{(+)}\rangle + |1D_{hh}^{(-)} 1D_e^{(-)}\rangle + |2S_{hh} 2S_e\rangle) \\ |\Psi_F\rangle &= \frac{1}{\sqrt{6}}(|1D_{hh}^{(+)} 1D_e^{(+)}\rangle + |1D_{hh}^{(-)} 1D_e^{(-)}\rangle - 2|2S_{hh} 2S_e\rangle) \end{aligned} \quad (5)$$

Here, the (\pm) labels indicate $L_z = \pm 1$ and ± 2 for the P and D states, respectively. The Coulomb interaction couples states $|\Psi_B\rangle$ and $|\Psi_H\rangle$. Thus the P - P transition is split in two lines $\Psi_a^{(s,p)} \simeq |\Psi_B\rangle + |\Psi_H\rangle$ and $\Psi_b^{(s,p)} \simeq |\Psi_B\rangle - |\Psi_H\rangle$. States $|\Psi_D\rangle$ and $|\Psi_F\rangle$, which arise from nominally allowed electron-hole configurations, are also coupled; consequently, the D - D transition splits in two lines $\Psi_a^{(d,d)} \simeq |\Psi_D\rangle + |\Psi_F\rangle$ and $\Psi_b^{(d,d)} \simeq |\Psi_D\rangle - |\Psi_F\rangle$. In contrast with atomistic models, in the 2D-EMA parabolic model the S - P and P - D single-particle level spacings are the same; so, the states $|\Psi_B\rangle$ and $|\Psi_H\rangle$ are degenerate, and so are $|\Psi_D\rangle$ and $|\Psi_F\rangle$. This symmetry-imposed degeneracy within the 2D-EMA model leads to significant Coulomb mixing in Eq. (5) that does not occur in our atomistic model, which lacks the imposed degeneracies of the parabolic confinement adopted in the 2D-EMA model. Consequently, the mixing enhancement $\eta(|\psi_H\rangle)$ within this model is ∞ (because transitions $2S_{hh}-1S_e$ and $1S_{hh}-2S_e$ are *forbidden* at the single-particle level).

To compare our atomistic predictions with the model calculations, we *deliberately neglect* in the

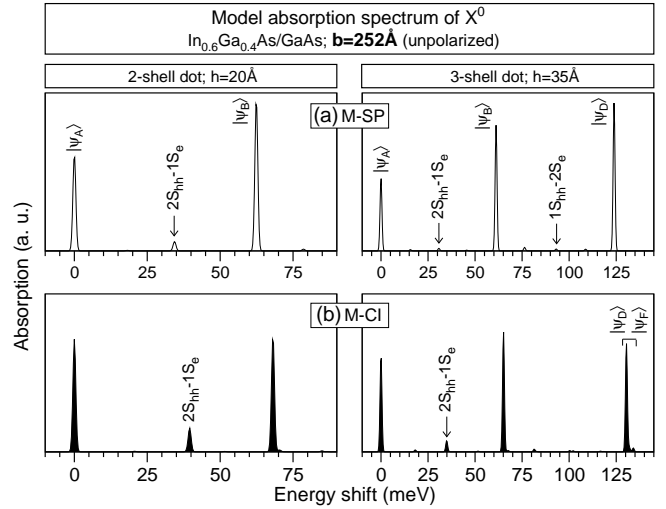


FIG. 4: Optical absorption spectrum of X^0 in two lens-shaped $\text{In}_{0.6}\text{Ga}_{0.4}\text{As}/\text{GaAs}$ quantum dots that confine two (left panel) and three (right) shells of electron states. In both cases, the spectra are calculated within a model single-particle (M-SP) [Eq. (2)] and configuration-interaction (M-CI) approach [Eq. (4)] (b), assuming degenerate $1P$, and $2D$ and $2S$ (in three-shell dot) electron and hole states but retaining the atomistic wavefunctions. Transitions are labeled following notation in Fig. 1 and Eq. (5). Vertical scales are different for each dot.

pseudopotential-based calculation the atomistic-induced splitting of the $1P$, and $1D$ and $2S$ states (but preserve their atomistically calculated wavefunctions). We calculate the absorption spectrum at the single-particle level [Eq. (2)] and separately in the many-particle approximation [Eq. (4)].^{24,25} Figures 4(a) and 4(b) show, respectively, the atomistic model calculation of the *single-particle* and *many-particle* absorption spectra. By comparing the results of Fig. 4 (atomistic wavefunctions; no P or D splittings) with the expectations from Eq. (5) (continuum wavefunctions; no P or D splittings), we find that (i) in the atomistic calculation the CI-enhanced transition corresponds to a mixture of states $|2S_{hh} 1S_e\rangle$ and $|\Psi_B\rangle$ instead of a mixture of $|\psi_H\rangle$ and $|\psi_B\rangle$ as in the model of Eq. (5); and (ii) the D -shell transition peak [$|\psi_D\rangle$, Fig. 4(a)] splits in two transitions that correspond to a mixture of $|\psi_D\rangle$ and $|\psi_F\rangle$ as in the 2D-EMA model. In turn, by comparing the results of Fig. 4 (atomistic wavefunctions; no P or D splittings) with Fig. 2 (atomistic wavefunctions *with* P and D splittings) we observe that transitions $1P_{hh}-1P_e$, and $1D_{hh}-1D_e$ and $2S_{hh}-2S_e$ are split; and several transitions appear above $1P_{hh}-1P_e$ in the 2-shell dot and in between the $1P_{hh}-1P_e$ and $1D_{hh}-1D_e$ transitions in the 3-shell dot.

Conclusion.—Atomistic, pseudopotential-based calculations of the excitonic absorption of lens-shaped $(\text{In},\text{Ga})\text{As}/\text{GaAs}$ quantum dots predict nontrivial spectra that show nominally-forbidden transitions enhanced by single-particle band-offset effects as well as many-body effects, and transitions involving deep, weakly con-

fined hole states with significant light-hole character. These transitions may explain the satellites of the P - P nominally-allowed transitions recently observed in PLE.

The authors thank G. Bester and L. He (NREL) for

valuable discussions, and V. Preisler (ENS, Paris) for making data available to them prior to publication. This work was funded by U.S. DOE-SC-BES-DMS, under Contract No. DE-AC3699GO10337 to NREL.

¹ A. Zunger, phys. stat. sol. (b) **224**, 727 (2001).

² L.-W. Wang *et al*, Phys. Rev. B **59**, 15806 (1999).

³ A. J. Williamson *et al*, Phys. Rev. B **62**, 12963 (2000).

⁴ P. Y. Yu and M. Cardona, *Fundamentals of Semiconductors—Physics and Materials Properties* (Springer, Berlin, 2003).

⁵ A. Franceschetti *et al*, Phys. Rev. B **60**, 1819 (1999).

⁶ Incoherent unpolarized light refers to unpolarized photons incoming from all directions.

⁷ G. A. Narvaez *et al*, J. Appl. Phys. **98**, 043708 (2005).

⁸ *Optical properties of semiconductor quantum dots*, U. Woggon (Springer-Verlag, Berlin, 1997).

⁹ G. A. Narvaez *et al*, Phys. Rev. B **61**, 13753 (2001).

¹⁰ P. Hawrylak *et al*, Phys. Rev. Lett. **85**, 389 (2000).

¹¹ F. Findeis *et al*, Solid State Comm. **114**, 227 (2000).

¹² U. Honester *et al*, Appl. Phys. Lett. **75**, 3449 (1999).

¹³ A. Vasanelli *et al*, Phys. Rev. Lett. **89**, 216804 (2002).

¹⁴ J.-B. Xia, Phys. Rev. B **40**, 8500 (1989).

¹⁵ H. Fu and A. Zunger, Phys. Rev. B **56**, 1496 (1997).

¹⁶ Band-mixing effects are responsible for mixing the $1S$ and $2S$ character of the single-particle hole states.

¹⁷ G. Bastard, *Wave Mechanics Applied to Semiconductor Heterostructures* (Halstead, New York, 1988).

¹⁸ P. R. C. Kent *et al*, Appl. Phys. Lett. **81**, 4377 (2002).

¹⁹ A. W. E. Minnaert *et al*, Phys. Rev. B **63**, 075303 (2001).

²⁰ E. Ribeiro *et al*, J. Appl. Phys. **87**, 7994 (2000).

²¹ F. Adler *et al*, J. Appl. Phys. **80**, 4019 (1996).

²² A. I. Akimov *et al*, Physica E **17**, 31 (2003); T. Flissikowski *et al*, Phys. Rev. B **68**, 161309(R) (2003).

²³ V. Preisler, private communication.

²⁴ Both dots confine more than three shells of hole states but we only consider three shells in this model calculation.

²⁵ In the pseudopotential-based plus CI calculation we do not use Eq. (5), but we let the Coulomb interaction mix the electron-hole configurations $|e_i h_j\rangle$ that compose the monoexciton states [Eq. (3)]. In addition, we include direct electron-hole Coulomb coupling but neglect the much smaller electron-hole exchange.